Identification of pyroptosis-related signature for cervical cancer predicting prognosis

Cankun Zhou[1], Chaomei Li[2], Yuhua Zheng[1], Xiaochun Liu[1,&]

[1]Department of Gynecology, Southern Medical University Affiliated Maternal and Child Health Hospital of Foshan, Foshan 528000, Guangdong, China
[2]Department of Maternity Centre, Southern Medical University Affiliated Maternal and Child Health Hospital of Foshan, Foshan 528000, Guangdong, China

Correspondence to: Yuhua Zheng, Xiaochun Liu; **email:** yuhuazhengcn@gmail.com, https://orcid.org/0000-0002-0977-5115; 2470650229@qq.com

ABSTRACT

Cervical cancer (CC) is one of the most common malignancies encountered in gynecology practice. However, there is a paucity of information about specific biomarkers that assist in the diagnosis and prognosis of CC. Pyroptosis is a form of programmed cell death whose different elements are related to the occurrence, invasion, and metastasis of tumors. However, the role of pyroptosis phenomena in the progression of CC has not yet been elucidated. This study focuses on the development of a pyroptosis-associated prognostic signature for CC using integrated bioinformatics to delineate the relationships among the signature, tumor microenvironment, and immune response of the patients. In this respect, we identified a prognostic signature that depends on eight pyroptosis-related genes (PRGs) that designate with better prognostic survival in the low-risk group (P<0.05) and where AUC values were greater than 0.7. A multi-factor Cox regression analysis indicated that such a signature could be used as an independent prognostic factor, and both the DCA and the Nomogram suggested that the proposed prognostic signature had good predictive capabilities. Interestingly, this prognostic signature can be applied to multiple tumors and thus, is versatile from a clinical point of view. In addition, there were significant differences in the tumor microenvironment and immune infiltration status between the high- and low-risk groups (P<0. 05). The core gene granzyme B (GZMB) was screened and the CC-associated regulatory axis, GZMB/ miR-378a/TRIM52-AS1, was constructed, which may promote CC progression, and further experimentation is needed to validate these results.

INTRODUCTION

Cervical cancer (CC) is the fourth most common type of malignancy that affects women across the world [1]. While the incidence and mortality rates of cervical cancer have declined significantly in high-income countries, the overall prognosis for CC patients in low-income countries remains poor [2, 3]. And in the event of recurrence and metastasis, the patient's prognosis is further reduced, so cervical cancer will remain a heavy burden of disease for a long time to come. Therefore, obtaining a lucid understanding of the molecular

mechanisms that underly the development of cervical cancer is crucial, and formulating methods for the early diagnosis and treatment is essential to improving the survival rate of CC patients.

Cell death is mainly divided into two categories, namely programmed death and non-programmed death. Programmed death mainly includes apoptosis, pyroptosis, and necroptosis, and non-programmed death mainly includes cell necrosis. Pyroptosis is a programmed cell death mechanism that is distinct from apoptosis and necrosis. It is mediated by the enzyme called caspase and

inflammasomes, and is characterized by a rapid plasma membrane rupture followed by the release of cellular contents and pro-inflammatory substances such as interleukins (IL). This triggers an inflammatory cascade that ultimately destroys the cell [4]. Pyroptosis not only plays an important role in infectious diseases, cardio-vascular diseases, and diseases that affect the central nervous system, but is also closely related to the development of tumors, for which it has both favorable and deleterious aspects [5]. On the one hand, when it is considered as an intrinsic immune mechanism, pyroptosis is a process that inhibits the occurrence and development of tumors. On the other hand, when considered as a type of pro-inflammatory cell death, pyroptosis provides a suitable microenvironment for tumor growth. The key elements that are involved in pyroptosis, such as inflammatory vesicles, gasdermin proteins, and pro-inflammatory cytokines, are also associated with the occurrence, invasion, and metastasis of tumors [6, 7]. Meanwhile, earlier studies have found that HeLa cells that overexpress gasdermin–B (GSDMB) exhibit evident pyroptosis characteristics [8]. Immune cells too, promote HeLa pyroptosis by releasing granzyme-B (GZMB) and lysing gasdermin-E (GSDME) [9]. In human papillomavirus (HPV)-positive cells, the expression of IL-1β, an important inflammatory molecule involved in pyroptosis, was completely inhibited. This effectively blocked the containment of tumor cells by pyroptosis. Meanwhile, the expression of SIRT1 in the CC cells affected the stability of the RelB mRNA, which in turn affected the expression of AIM2. When SIRT1 was knocked down, the RelB stability was enhanced significantly and the expression of the inflammation-related AIM2 genes wasup-regulated, triggering AIM2 inflammation vesicle-mediated pyroptosis [10, 11]. However, the characterization and determination of the prognostic value of PRGs for CC has not yet been completed.

In this study, we analyzed the genetic data of cervical cancer in the TCGA (The Cancer Genome Atlas) database and the UCSC Xena database to describe the expression levels and genetic changes of PRGs, and constructed and validated a prognostic model based on CC samples, and screened out core genes and pan-cancer analysis.

MATERIALS AND METHODS

Datasets and preprocessing

The TCGA database (https://portal.gdc.cancer.gov/) and the UCSC Xena database (https://xena.ucsc.edu/) were used to obtain CC data. Our research program was shown in Supplementary Figure 1. The RNA sequence data, clinicopathological parameters, and genomic mutation data (including somatic mutations and copy number variants (CNV)) were obtained for 306 CC tissues and 3 paraneoplastic tissue samples. Based on earlier studies [9, 12, 13], 35 PRGs were included, namely AIM2, CASP1, CASP3, CASP4, CASP5, CASP6, CASP8, CASP9, ELANE, GPX4, GSDMA, GSDMB, GSDMC, GSDMD, GSDME, GZMA, GZMB, IL18, IL1B, IL6, NLRC4, NLRP1, NLRP2, NLRP3, NLRP6, NLRP7, NOD1, NOD2, PJVK, PLCG1, PRKACA, PYCARD, SCAF11, TIRAP, and TNF, as detailed in Supplementary Table 1. Comparison of mRNA expression levels of PRGs in paraneoplastic tissue and CC tissues, and visualization of somatic mutations and CNV in CC tissues by the R software 'maftools' and the 'Rcircos' package. The Kaplan Meier-Plotter online platform (https://kmplot.com/analysis/) was used to further analyze the survival and prognosis of PRGs [14]. All subsequent statistical analyses were performed via R version 4.0.2. The screening criterion for differential expression of PRGs was P<0.05.

Establishment of prognostic signature

The data for 304 CC patients were obtained from the TCGA database and used as the training dataset to screen for prognosis-related PRGs and exclude samples with no survival time. We constructed a prognostic signature for the PRGs using a univariate Cox proportional regression analysis and the least absolute shrinkage and selection operator (Lasso) regression, which was stratified according to the risk score (Risk score = $EXP_{PRGs\ 1} \times Coefficient_1 + EXP_{PRGs\ 2} \times Coefficient_2 + ... + EXP_{PRGs\ n} \times Coefficient_n$). Subsequently, the associated risk score was calculated for each patient in the training dataset. Based on the median score, the patient's data were grouped as low or high risk. The difference in survival between the two groups was determined using the log-rank test and the Kaplan-Meier curves, while the sensitivity and specificity of the prognostic signature were determined from the ROC curves plotted using the 'survivalROC' package. To determine the feasibility and reliability of the proposed prognostic signature, the training dataset of CC patients (N = 304) was randomly divided into test datasets A (N = 152) and B (N = 152) using the 'Caret' package. Subsequently, the same statistical methods were used for validating both test datasets.

Then, independent prognostic analyses and decision curve analysis (DCA) were performed to combine the clinical features, and a nomogram was constructed to predict the one-, three- and five-year survival rates of CC patients to assess the prognostic value of the signature.

The TCGA pan-cancer transcriptional expression data and clinical data were obtained from the Xena database

that includes 33 cancer types, as detailed in Supplementary Table 2. The prognostic model was applied to the remaining 32 tumors to analyze their prognostic outcomes for the different cancers. The risk score was considered to be significantly associated with CC patient survival when p<0.05.

Tumor mutation burden, tumor microenvironment, and immune cell infiltration analysis

Tumor mutation burden (TMB) is a biomarker that can predict how a patient might respond to immunotherapy [15]. Differences in TMB between the high and low-risk groups were compared based on original data of somatic mutations in CC patients, and the risk scores and TMB were compared using the Spearman correlation analysis. An ESTIMATE algorithm was used to predict the purity of the CC [16], and the proportion of stromal cells (stromal score) and immune cells (immune score) that have infiltrated the tumor tissue as well as the measured differences in the tumor microenvironment (TME) between the two risk groups were assessed.

Immune cell infiltration data from CC were obtained from the Timer 2.0 database (http://timer.cistrome.org/) [17]. Four algorithms were eventually chosen [18–20], including TIMER, CIBERSORT, QUANTISEQ, and MCPCOUNTER, according to the PRG signature, and the correlation between the immune cell infiltration and risk score under different algorithms was analyzed using Spearman correlation and represented as a bubble plot. In addition, the differences in immune function, HLA gene expression, immune checkpoint, and m6A gene expression were compared for the high- and low-risk groups using the Wilcox test. P < 0.05 was considered to be statistically significant.

Construction of mRNA-miRNA-lncRNA interaction network

To screen for the relevant genes in the prognostic signature, we searched for protein-protein interactions (PPI) via the String (https://string-db.org/) online database. The degrees of connectivity of these PRGs were also counted. Next, the correlations of genes in the PRG signature were evaluated concerning the clinical feature 'Grade'. The patients were divided into two subgroups, namely, G1-2 and G3-4, and the Wilcox test was used for their analysis. The genes with the highest connectivity and statistically significant correlation with 'Grade' in the signature were designated as the core genes.

Then, pan-cancer differential analysis, survival analysis, and TMB correlation analysis were performed on these core genes that were designated in the previous step. We used boxplots to summarize the overall levels of expression of the core gene in the 33 TCGA cancer samples. Based on 18 types chosen from more than five adjacent normal tissues, a linear mixed-effect model was used to compare and analyze the difference in gene expression between the tumor and the paracancerous tissues. The TMB scores were obtained from UCSC Xena database. Correlation analysis between the core gene expression and TMB was performed using Spearman's method. A forest plot was drawn to determine whether the expression of the core gene correlated with the patient survival obtained by the univariate Cox analysis.

To construct the mRNA-miRNA-LncRNA interaction network for the core genes, the miRNAs targeted by the core genes were predicted using the TargetScan (http://www.targetscan.org/vert_72/) and miRTarBase (http://mirtarbase.cuhk.edu.cn/) databases. The predicted miRNAs were intersected. Subsequently, the differential expression levels and prognostic values of these miRNAs were analyzed. Based on the prognosis and differentially expressed miRNAs, LncBase Predicted v.2 (https://carolina.imis.athena-innovation.gr/diana_tools/web/index.php?r=lncbasev2/index-predicted) and StarBase (http://starbase.sysu.edu.cn/) were used to predict the LncRNAs that the miRNAs might eventually bind. The differential expression levels and prognostic value of these LncRNAs were analyzed in detail, and on this basis, we constructed the mRNA-miRNA-LncRNA interaction networks. The statistically significant difference was P < 0.05.

Availability of data and materials

The information of this study is obtained by the TCGA, UCSC Xena, Kaplan Meier-Plotter, Timer 2.0, String, TargetScan, miRTarBase, LncBase Predicted v.2, and StarBasedatabase database. We are grateful to them for the source of data used in our study.

RESULTS

Genetic variation profile of PRGs in CC

First of all, we found that the AIM2, CASP3, CASP4, CASP5, CASP6, CASP8, GSDMB, GSDMC, GZMB, IL18, NLRP2, NLRP7, NOD2, PYCARD, and TNF were significantly up-regulated in CC tissues, while ELANE, NLRP1, NOD1, and PJVK were significantly down-regulated (Figure 1A). A survival prognosis analysis showed that IL 1B and PRKACA had a significant correlation with the prognosis of CC patients. Those patients with low expression of IL 1B and high expression of PRKACA have a better prognosis for

survival (Figure 1B, 1C). Figure 1D shows the locations of the CNV alterations on the PRG chromosomes, and it can be observed that CNV changes were prevalent in these genes. PRKACA had the highest probability of CNV amplification and GPX4 had the highest frequency of CNV deletion (Figure 1E). The somatic mutations of these PRGs in CC were also analyzed and it was concluded that the overall mutation frequency was not high in these cases (≤4%) (Figure 1F).

Construction and evaluation of the effectiveness of prognostic signature

A survival analysis of the PRGs in the training dataset was conducted via a univariate Cox proportional regression model and screened for eight PRGs that had prognostic value (Figure 2A). Among these, GZMB and TNF were expressed in high level in CC tissue while NOD1 was significantly low (Supplementary Figure 2B).
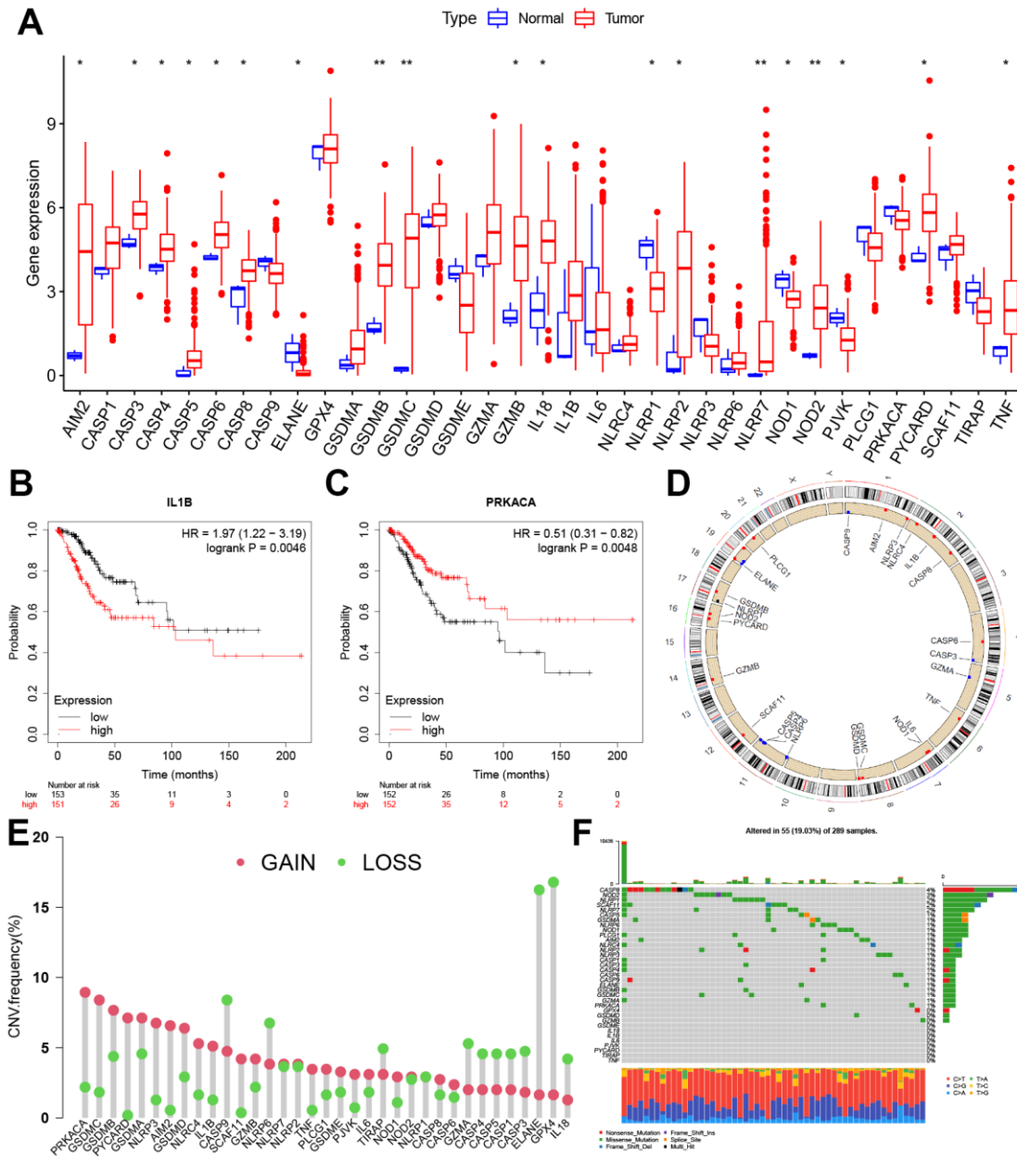

Figure 1. Expression and genetic variation landscape of PRGs in CC. (**A**) The boxplot demonstrated the expression of PRGs between normal and CC samples. Patients with low expression of IL 1B (**B**) and high expression of PRKACA (**C**) have more survival benefits. (**D**) Location of CNV alterations in PRGs on 23 chromosomes in CC cohort. (**E**) The CNV variation frequency of PRGs. The red and green dots represent CNV amplification and deletion, respectively. (**F**) Genetic alteration on a query of PRGs. PRGs, Pyroptosis-related genes. CC, Cervical cancer. CNV, Copy number variation. *p < 0.05, **p < 0.01, and ***p < 0.001.

Following this, the pyroptosis-related signature was constructed by further downscaling the prognosis-related PRGs via Lasso regression (Figure 2B, 2C). The risk score was calculated for each patient using the expression, risk score= $(-0.0037 \times EXP_{GPX4})$ + $(0.0377 \times EXP_{GSDME})$ + $(-0.0043 \times EXP_{GZMA})$ + $(-0.026 \times EXP_{GZMB})$ + $(0.0017 \times EXP_{IL1B})$ + $(0.4741 \times EXP_{NOD1})$ + $(-0.1298 \times EXP_{PRKACA})$ + $(0.0642 \times EXP_{TNF})$. According to the median, the patients were divided into low-risk and high-risk groups, and the survival prognostic analysis showed a significant survival benefit for patients classified as low-risk (P < 0.001, Figure 3A), with an AUC value of 0.789 (Figure 3D). In test datasets A and B, the difference in survival prognosis (P < 0.05, Figure 3B, 3C) and predictive efficacy (AUC values of 0.707 and 0.943, respectively, Figure 3E, 3F) were validated
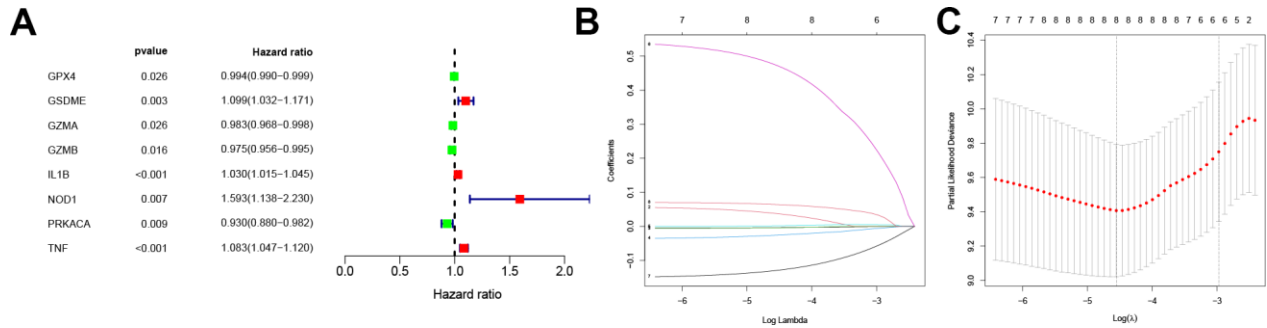
Figure 2. Screening for prognosis-related PRGs and LASSO regression. (**A**) Forest plot of the prognosis-related PRGs based on P < 0.05. Red and green indicate high and low risk, respectively. (**B**) LASSO coefficients for PRGs. Each curve represents a PRGs. (**C**) 1,000-fold cross-validation of variable selection in LASSO regressions by 1-SE criteria. PRGs, Pyroptosis-related genes. LASSO, Least absolute shrinkage and selection operator.
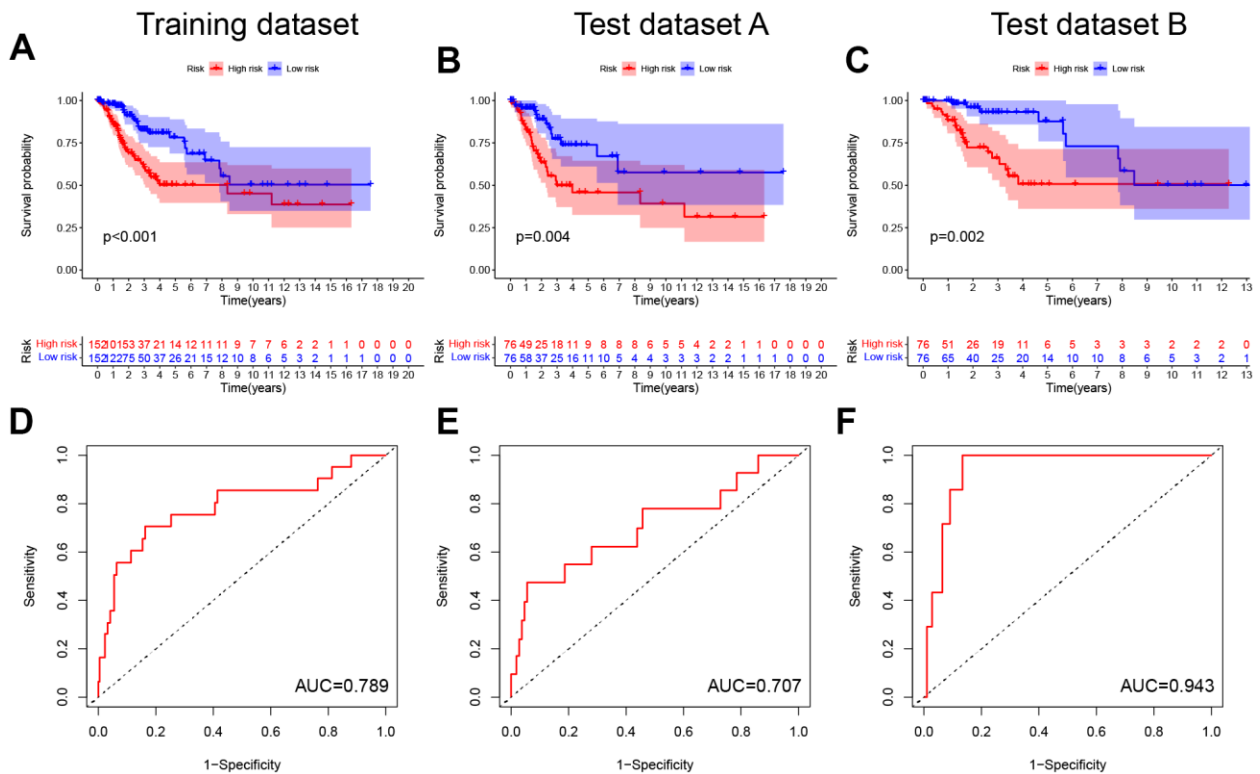
Figure 3. Construction and validation of the pyroptosis-related signature. (**A**–**C**) Kaplan-Meier curves showed lower overall survival rates in the high-risk group than in the low-risk group in the training dataset, test dataset A and test dataset B (P < 0.05). (**D**–**F**) The predicted ROC curves for the training dataset, test dataset A and test dataset B were 0.789, 0.707, and 0.943 respectively.

similarly, thereby confirming the overall accuracy and validity of the prognostic signature. Interestingly, this prognostic model indicated a better prognosis for patients in the low-risk group than in the high-risk group in glioblastoma multiforme (GBM), brain lower grade glioma (LGG), liver hepatocellular carcinoma (LIHC), and uterine corpus endometrial carcinoma (UCEC) (Supplementary Figure 3).

Univariate and multivariate COX analyses in conjunction with the patient age, stage, and grade, showed that this pyroptosis-related signature was an independent prognostic factor for OS in CC patients (p < 0.001, Figure 4A, 4B). In addition, the risk score corresponded to the highest AUC value (AUC = 0.794, Figure 4C) compared to other clinical features. The DCA further demonstrated the clinical usefulness of the signature (Figure 4D). The Nomogram for both the signature and clinical features was stable and accurate, and it can be used to predict the one-year, three-year, and five-year survival rates in CC patients (Figure 4E).

Correlation of TMB, TME, and immune cell infiltration with prognostic signature

Previous studies have indicated the crucial role of TME in the occurrence and development of tumors [21]. As TMB predicts patient response to immunotherapy, our study found that patients in the high-risk group typically had low TMB scores, and the risk score was negatively correlated with the TMB score to a significant extent. The results of the survival analysis showed that patients that scored high on risk and low on TMB possessed a significant survival advantage (Figure 5A–5C). Compared to the high-risk group, the ESTIMATEScore, ImmuneScore, and StromalScore were all higher in the low-risk group (Figure 5D).

The relation between the immune response and risk score based on the TIMER, QUANTISEQ, MCPCOUNTER, and CIBERSORT algorithms is shown in Figure 5E. The risk score was negatively correlated to the infiltration levels of B cells, T cell
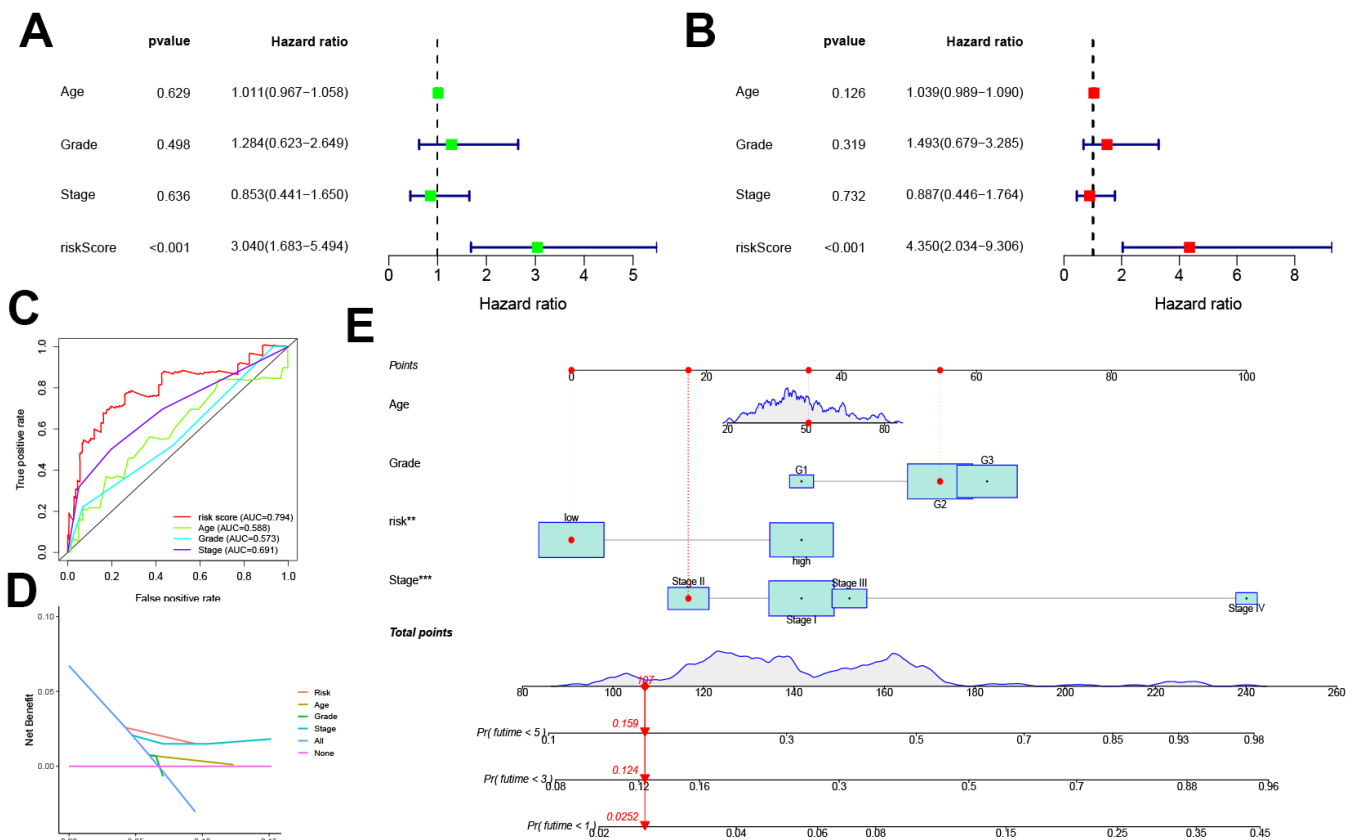
Figure 4. Prognostic value of the pyroptosis-related signature. (**A**, **B**) Univariate and multivariate COX analysis for the prognostic signature and clinical features (including Age, Stage, and Grade). (**C**) The AUC values of the prognostic signature and clinical features. (**D**) The DCA of the prognostic signature and clinical features. (**E**) Nomogram for both the signature and clinical features to predict one-, three- and five-year survival rates.

CD8+, and macrophages, and positively correlated to the infiltration level of neutrophils. The analysis of immune function differences showed that mechanisms such as the antigen-presenting cell (APC) co-inhibition/ APC_co_stimulation, CC chemokine receptor (CCR), check-point, cytolytic_activity, human leukocyte antigen (HLA), Inflammation promotion, and T cell co-inhibition/ stimulation were significantly more active in the low-risk group (Figure 6A).

Considering this analysis of the immune function, the levels of HLA-related gene expression l were further studied as shown in Figure 6B. The levels of expression of HLA-DMA, HLA-DQB1, HLA HLA-DMA, HLA-DQB1, HLA-DRA, etc. were significantly higher in the low-risk group. As checkpoint inhibitors are crucial to immunotherapy, the differences in immune checkpoint expression between the two groups were analyzed in detail. Significant differences were demonstrated in the expression of PDCD1LG2, TMIGD2, CD27, CD40LG, etc. for the two groups (Figure 6C). Recent research suggests that m6A can regulate the immune response

and also modify the immune microenvironment of the tumor [22]. On comparing the m6A-related expression of mRNA between the high- and low-risk groups, it was seen that YTHDF3 and LRPPRC ad significantly high levels of expression in the high-risk group (Figure 6D)

Construction of mRNA-miRNA-lncRNA interoperability network

The interrelationships between the 35 PRGs considered in this study were retrieved from the STRING database and a PPI network having a composite score of > 4.0 was constructed. A complex, close-knit network of interrelationships was found among these genes was determined (Supplementary Figure 4A). Subsequently, the degree of connectivity between these genes (Supplementary Figure 4B). We further examined the relationship between levels of mRNA expression in the pyroptosis-related signature and CC grade staging, and found that the expressions of GPX4, GZMA, and GZMB were significantly higher in the G3-4 group compared to the G1-2 group (P < 0.05, Supplementary Figure 4C–4F).
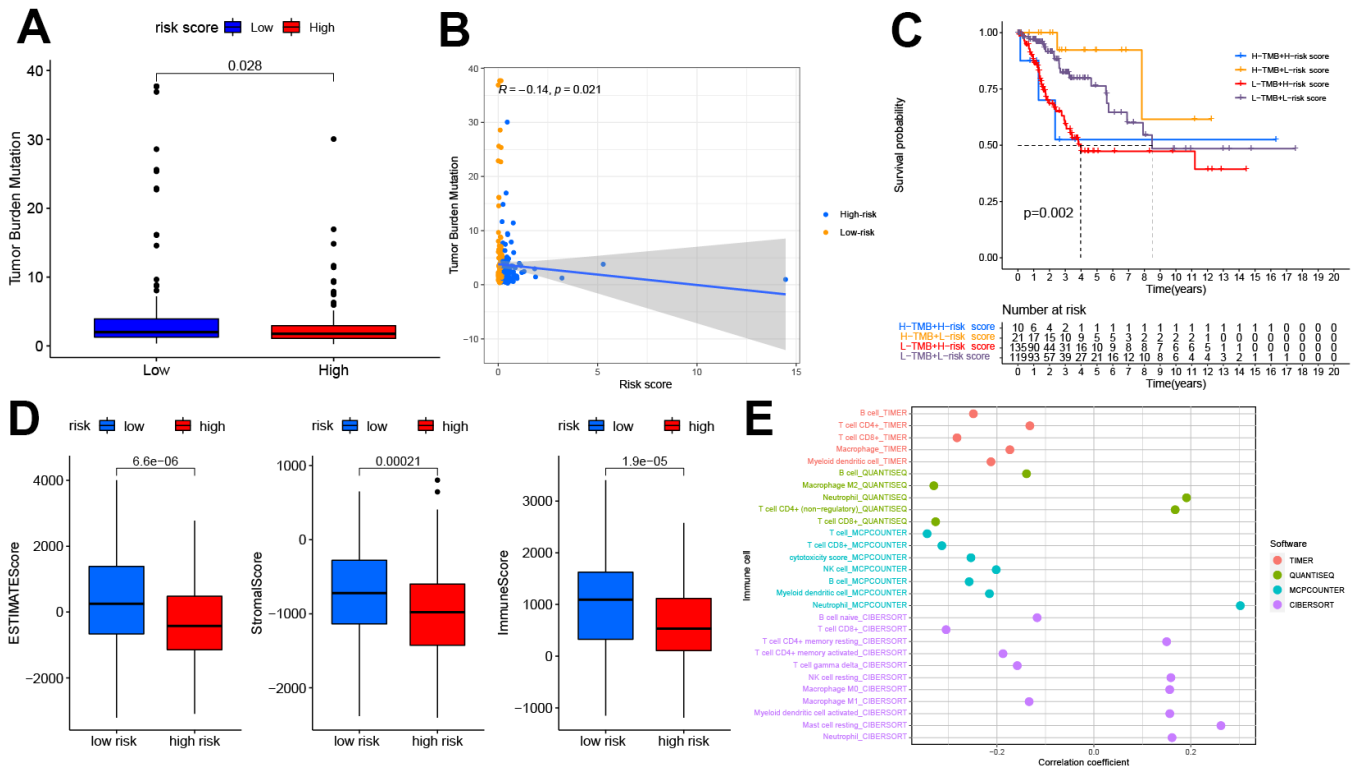

Figure 5. The relationship between the pyroptosis-related signature and the TMB, TME, and immune cell infiltration. (**A**) Patients in the high-risk group had lower TMB (P<0.05). (**B**) The correlation between risk score and TMB (R=-0.14, P<0.05). (**C**) Kaplan-Meier curves showed lower overall survival rates in the low-TMB combined with the high-risk group than in the other three groups(P<0.05). (**D**) The relationship between the risk score and TME, patients in the high-risk group had the lower stromal score, immune score, and estimate score(P<0.05). (**E**) The relationship between the risk score and immune cell infiltration is based on TIMER, QUANTISEQ, MCPCOUNTER, and CIBERSORT algorithm. Bubble plot for immune responses significantly associated with a risk score. TMB, tumor mutation burden. TME, tumor microenvironment.

Moreover, the degree of connectivity of GPX4, GZMA, and GZMB in the PPI network above was 4, 4, and 10, respectively, suggesting that GZMB may indeed be involved in tumor growth and progression in CC patients.

Pan-cancer expression analysis was performed for GZMB, which showed its significantly high expression in cholangiocarcinoma (CHOL), colon adenocarcinoma (COAD), esophageal carcinoma (ESCA), glioblastoma multiforme (GBM), head and neck squamous cell carcinoma (HNSC), kidney renal clear cell carcinoma (KIRC), rectum adenocarcinoma (READ), stomach adenocarcinoma (STAD), and UCEC tissues, while significantly low expression was observed in lung adenocarcinoma (LUAD) and lung squamous cell carcinoma (LUSC) tissues (Figure 7A). TMB is a biomarker that indicates response to immunotherapy, and so, the relation between the expression of GZMB and TMB was investigated. The levels of expression of GZMB were significantly and positively correlated with TMB in bladder urothelial carcinoma (BLCA), breast invasive carcinoma (BRCA), cervical squamous cell carcinoma, and endocervical adenocarcinoma (CESC orCC), CHOL, COAD, LGG, LUAD, STAD, and UCEC, Meanwhile, the correlation was significantly negative with kidney renal papillary cell carcinoma (KIRP) and thyroid carcinoma (THCA) (Figure 7B). Interestingly, the cases of CHOL, COAD, STAD, and
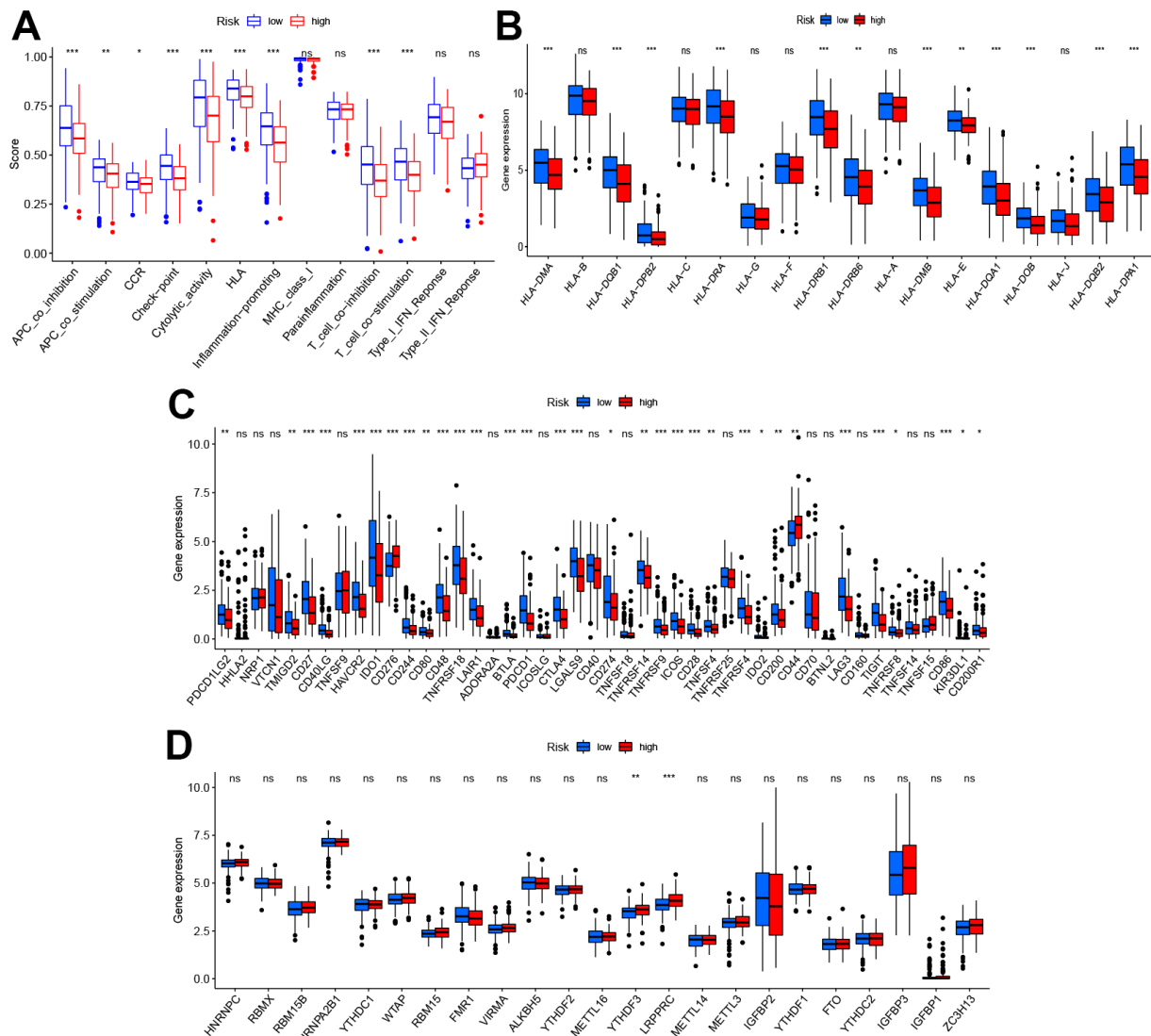

Figure 6. Diversity of immune microenvironment characteristics in high- and low-risk groups. (A) The activity differences of each immune function between high and low-risk groups. (B) The differences of each HLA-related gene between both risk groups. (C) The expression status of immune checkpoints between both risk groups. (D) The expression status of m6A-related genes between both risk groups. *p < 0.05, **p < 0.01, and ***p < 0.001.

UCEC in the high-GZMB-expression group also had high TMB values, and these are expected to be more sensitive to immunotherapy. In contrast, LUAD in the low expression group had low TMB values and so, may be resistant to cell scorch-related immunotherapy. Prognostic correlation analysis showed that the GZMB was negatively correlated with survival in BLCA, BRCA, CESC, ovarian serous cystadenocarcinoma (OV), skin cutaneous melanoma (SKCM), UCEC, and uveal melanoma (UVM). Meanwhile, it was positively correlated with GBM, KIRC, KIRP, acute myeloid leukemia (LAML), and LGG (P<0.05, Figure 7C).
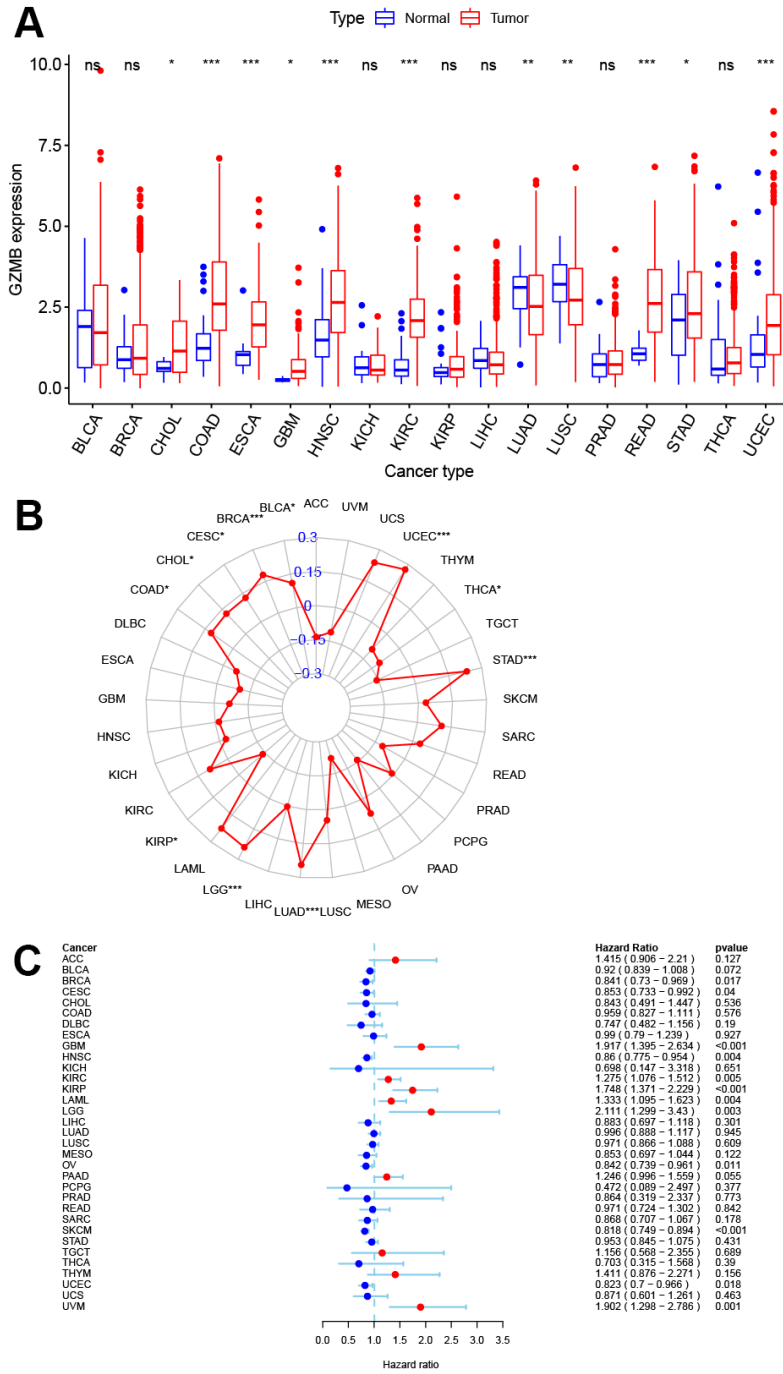

Figure 7. Pan-cancer analysis of core gene GZMB expression and survival prognosis. (**A**) Boxplot of GZMB differential expression between cancer and adjacent normal tissues. (**B**) Radar graph indicating the correlation between the GZMB expression and TMB in pan-cancer by Spearman's method. (**C**) Expression of GZMB correlates with overall survival in patients with different cancer types using univariate Cox proportional hazard regression models. *p < 0.05, **p < 0.01, and ***p < 0.001.

To elucidate the potential molecular regulation mechanism of GZMB in CC, we further constructed an mRNA-miRNA-LncRNA interaction network. First, based on the comprehensive prediction using the TarBase and mirTarBase databases, we screened out miRNAs that can target and regulate the GZMB core gene, and subsequently, ten miRNAs were obtained by considering the intersection (Figure 8A). Further analysis showed that miR-378a was significantly upregulated in CC (Figure 8B) and patients who show a high expression have a better prognosis for survival (Figure 8C). The LncRNA targets upstream of miR-378a were obtained from the LncBase and StarBase databases, and a total of five LncRNAs (Figure 8D) were obtained by intersection to finally construct the mRNA-miRNA-LncRNA inter-

action network (Figure 8E). Subsequently, these five LncRNAs were subjected to differential expression analysis and survival prognosis analysis, which showed that TRIM52-AS1 was significantly downregulated in CC (Figure 8F), and its high level of expression indicated a considerable survival advantage (Figure 8G). Thus, it may be concluded that the GZMB/miR-378a/TRIM52-AS1 regulatory axis plays an important regulatory role in the development of CC.

DISCUSSION

Pyroptosis is a type of programmed cell death that plays a dual role in the occurrence and development of tumors. It can regulate cell morphology, proliferation,
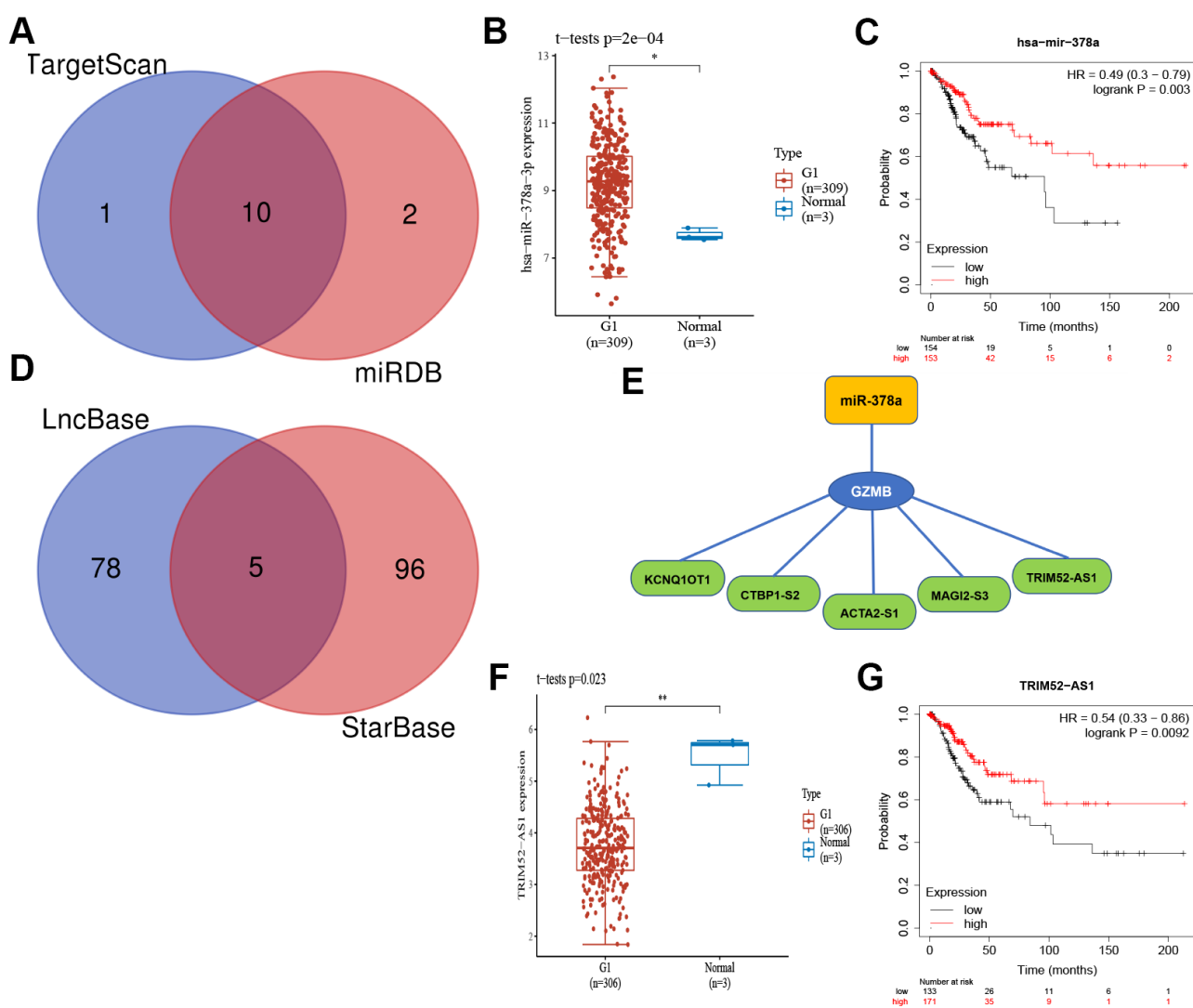
Figure 8. The core gene GZMB associated mRNA-miRNA-lncRNA interaction network construction. (**A**) Venn diagram of miRNAs of TarBase and mirTarBase. The expression (**B**) and prognostic value (**C**) of miR-378a (Synonyms: has-miR-378a-3p) in CC patients. (**D**) Venn diagram of LncRNAs of LncBase and StarBase. (**E**) Regulatory network mRNA-miRNA-Lnc-RNA. The expression (**F**) and prognostic value (**G**) of TRIM52-AS1 in CC patients. CC, Cervical cancer.

infiltration, migration, and chemotherapy resistance through a variety of cell signaling pathways, thereby influencing tumor progression, and may be associated with patient prognosis [5]. However, the regulatory mechanisms and networks that link pyroptosis and CC are not fully understood. Our study aims to elucidate this aspect and paths that can be used for developing interventions.

In terms of gene expression, we first found that genes AIM2, CASP3, CASP4, CASP5, CASP6, CASP8, GSDMB, GSDMC, GZMB, IL18, NLRP2, NLRP7, NOD2, PYCARD, and TNF were chiefly up-regulated in CC tissues, while the genes ELANE, NLRP1, NOD1, and PJVK were down-regulated. Among these, those CC patients who had low IL 1B expression and high PRKACA expression had poorer survival rates. This is consistent with earlier findings that indicate that these PRGs are closely associated with tumor development. In cervical, gastric, and colorectal cancers, high IL-1B expression has been associated with shorter patient survival [23, 24]. In addition, it has been noted that IL-1β expression was elevated in prostate cancers that show a high tendency to metastasize [25]. During their study of head and neck tumors, Dong et al. found a considerable increase in lymph node metastasis with increased IL-1β expression [26]; this indicated that high IL1B expression is detrimental to the survival of tumor patients. Many studies have shown that PRKACA is crucial to the development and progression of a variety of cancers [27], and also that it can be used as a biomarker for hepatocellular carcinoma [28]. Therefore, these genes have the potential to be new molecular targets for CC.

In ovarian and gastric cancers, researchers have identified PRGs and also constructed and validated several prognostic models for them [13, 29]. Hence, a pyroptosis-related signature was formulated, which consisted of eight PRGs with prognostic value (GPX4, GSDME, GZMA, GZMB, IL1B, NOD1, PRKACA, TNF); the univariate Cox proportional risk regression and Lasso regression were used, where patients in the low-risk group had better prognosis of survival. The signature could effectively predict the prognosis for CC patients (AUC > 0.7), and several independent prognostic analyses have shown that this signature can be considered as an independent prognostic factor. The associated nomogram has shown to be stable and accurate, and therefore can be used satisfactorily to predict survival at one, three, and five years in CC patients, presenting additional options for prognosis prediction in CC.

Another important finding indicates that this prognostic model has a significant relation with the TME, which confirms that pyroptosis plays a notable role in the TME. A mounting body of evidence shows that cell death by pyroptosis is particularly important for the formation of tumors and TME, and it has a more marked effect on the immune microenvironment of the tumor [30]. Studies have confirmed that approximately 95% of cervical cancer cases may be caused by persistent HPV infections. Consequently, the human immune system plays an important role in the body's infection response process, thus laying the foundation for the immunotherapy of cancer [31].

This was confirmed in our study, which determined significant differences in TME and immune function between the low- and high-risk groups. It was found that patients with high TME scores had a better prognosis. This finding is consistent with previous studies that concluded that patients with high TME scores exhibited a stronger anti-tumor immune response, stood to benefit more from immunotherapy, and survive longer [32, 33]. In addition, the correlation analysis showed that the B cell and T cell CD8+ correlated negatively with the risk scores, while neutrophils correlated positively with them. Recent studies have shown that the gene GSDME is a tumor suppressor that can enhance the phagocytosis of tumor-associated macrophages and promote the infiltration and activation of NK cells and CD8+ T lymphocytes, thereby inhibiting tumor growth [9]. Xi et al. found that GSDMD was positively correlated with the expression levels of CD8A, GZMB, and IFNG in non small cell lung cancer (NSCLC) tissues, and the expression was up-regulated in activated CD8+ T cells. This enhanced the lethality of CD8+ T cells towards the NSCLC cells [34]. Consistent with this result, Wang et al. found that when a bio-orthogonal shear system was applied to gasdermin protein activated pyroptosis, it reshaped the tumor immune microenvironment of the tumor and activated a strong T cell-mediated anti-tumor immune response that exerted a powerful anti-tumor effect [35]. It was also observed that tumor-associated neutrophils are involved in regulating tumor development, while IL-1β and IL-18 route neutrophils to tumor sites [36]. Meanwhile, GSDMD induces neutrophil death [37]. Neutrophils may be involved in the local and systemic triggering of immune escape in cervical cancer cells. An increase in the total neutrophil count in progressive cervical cancer reduces the anti-tumor activity of T cells and suppresses thereby suppressing the immune action [38–40]. At the same time, our study confirmed that the expression of multiple immune checkpoints and m6A-related mRNAs showed considerable difference between the low- and high-risk groups. Later studies have found that the abnormal expression of the immune checkpoints affects the immune microenvironment of the tumor and helps tumor cells evade the body's

immune response [41, 42]. These studies unequivocally indicate that the host immune response and micro-environment are closely related to the progression of CC.

In our study, GZMB, which is a component of the prognostic model, was significantly upregulated in CC tissues. That is, GZMB expression was significantly up-regulated in patients with advanced (grade 3 and grade 4) CC, while it was negatively associated with survival. GZMB is a serine protease and a pro-inflammatory molecule that promotes the progression of inflammatory diseases and cancers [43]. It is expressed in uroepithelial carcinoma, pancreatic cancer, and melanoma cells, and is known to promote cancer cell invasion [44–46]. Our study also found that GZMB was negatively associated with survival in both BLCA and SKCM. For a long time, GZMB has been established as being influential in protein hydrolysis-mediated apoptosis, while its role in pyroptosis has not been given due attention. GZMB was found to be able to cleave GSDME and kill lymphocytes to activate the process of pyroptosis, thus changing apoptosis to pyroptosis [9].

The GZMB/miR-378a/TRIM52-AS1 regulatory axis that has a strong correlation to the development of CC was extracted from the mRNA-miRNA-LncRNA interaction network. MicroRNA-378a (miR-378a, previously known as miR-378) is an important small molecule that belongs to the non-coding RNA family. The aberrant up-regulation of miR-378a in HPV16/18 positive cervical cancer tissues has been reported earlier. The expression of miR-378a may be elevated by the action of oncoprotein E6/E7 [47]. ElevatedmiR-378a expression has also been reported in cervical cancer tissues and cell lines, and may act through the ST7L/Wnt/β-catenin signaling pathway [48]. At present, there is a paucity of investigations regarding the regulation of TRIM52-AS1 in tumors. For example, the down-regulation of TRIM52-AS1 inhibited the proliferation and migration of renal cell carcinoma (RCC) cells and promoted apoptosis in them. Studies on hepatocellular carcinoma (HCC) have shown that the TRIM52-AS1 knockdown inhibits the proliferation and metastasis of HCC cells. TRIM52-AS1 behaves as a competitive endogenous RNA (ceRNA) and promotes the progression of HCC by sponging the miRNAs and up-regulating the expression of the mRNAs that are regulated by miRNAs [49, 50]. Therefore, it can be concluded that TRIM52-AS is down-regulated in CC tissues; this attenuates the sponging effect on miR-378a, and increases the binding of miR-378a to GZMB, which in turn inhibits and down-regulates the expression of GZMB. This agrees with our findings that the overall survival was significantly lower in the group that showed low-TRIM52-AS1 expression than in the group

with high-TRIM52-AS1 expression (Figure 8G) in CC patients. Moreover, the lower the expression of GZMB as a protective factor (Figure 7C), the worse the prognosis was; thus, TRIM52-AS1 may be concluded to promote the progression of cervical cancer through miR-378a/GZMB, which needs to be studied further for validation.

In conclusion, we formulated an effective prognostic signature and constructed a GZMB/miR-378a/TRIM52-AS1 regulatory axis based on several PRGs. This is expected to be relevant in the theoretical study of molecular mechanisms and for assessing the prognosis of cervical cancer patients. However, our study has some limitations. Tumor heterogeneity has not been considered in this study although it cannot be overlooked and must be validated by more extensive *in-vivo* and *in-vitro* studies.

AUTHOR CONTRIBUTIONS

Cankun Zhou and Yuhua Zheng performed data analysis work and aided in writing the manuscript. Cankun Zhou and Xiaochun Liu designed the study, assisted in writing the manuscript. Chaomei Li edited the manuscript. All authors read and approved the final manuscript.

CONFLICTS OF INTEREST

The authors declare that they have no conflicts of interest.

Editorial note

&This corresponding author has a verified history of publications using a personal email address for correspondence.

REFERENCES

1. Ward ZJ, Grover S, Scott AM, Woo S, Salama DH, Jones EC, El-Diasty T, Pieters BR, Trimble EL, Vargas HA, Hricak H, Atun R. The role and contribution of treatment and imaging modalities in global cervical cancer management: survival estimates from a simulation-based analysis. Lancet Oncol. 2020; 21:1089–98.
https://doi.org/10.1016/S1470-2045(20)30316-8
PMID:32758463

2. Cohen PA, Jhingran A, Oaknin A, Denny L. Cervical cancer. Lancet. 2019; 393:169–82.
https://doi.org/10.1016/S0140-6736(18)32470-X
PMID:30638582

3. Ward ZJ, Scott AM, Hricak H, Atun R. Global costs,

health benefits, and economic benefits of scaling up treatment and imaging modalities for survival of 11 cancers: a simulation-based analysis. Lancet Oncol. 2021; 22:341–50.
https://doi.org/10.1016/S1470-2045(20)30750-6
PMID:33662286

4. Karki R, Kanneganti TD. Diverging inflammasome signals in tumorigenesis and potential targeting. Nat Rev Cancer. 2019; 19:197–214.
https://doi.org/10.1038/s41568-019-0123-y
PMID:30842595

5. Zheng Z, Li G. Mechanisms and Therapeutic Regulation of Pyroptosis in Inflammatory Diseases and Cancer. Int J Mol Sci. 2020; 21:1456.
https://doi.org/10.3390/ijms21041456
PMID:32093389

6. Rathinam VA, Fitzgerald KA. Inflammasome Complexes: Emerging Mechanisms and Effector Functions. Cell. 2016; 165:792–800.
https://doi.org/10.1016/j.cell.2016.03.046
PMID:27153493

7. Kolb R, Liu GH, Janowski AM, Sutterwala FS, Zhang W. Inflammasomes in cancer: a double-edged sword. Protein Cell. 2014; 5:12–20.
https://doi.org/10.1007/s13238-013-0001-4
PMID:24474192

8. Zhou Z, He H, Wang K, Shi X, Wang Y, Su Y, Wang Y, Li D, Liu W, Zhang Y, Shen L, Han W, Shen L, et al. Granzyme A from cytotoxic lymphocytes cleaves GSDMB to trigger pyroptosis in target cells. Science. 2020; 368:eaaz7548.
https://doi.org/10.1126/science.aaz7548
PMID:32299851

9. Zhang Z, Zhang Y, Xia S, Kong Q, Li S, Liu X, Junqueira C, Meza-Sosa KF, Mok TM, Ansara J, Sengupta S, Yao Y, Wu H, Lieberman J. Gasdermin E suppresses tumour growth by activating anti-tumour immunity. Nature. 2020; 579:415–20.
https://doi.org/10.1038/s41586-020-2071-9
PMID:32188940

10. So D, Shin HW, Kim J, Lee M, Myeong J, Chun YS, Park JW. Cervical cancer is addicted to SIRT1 disarming the AIM2 antiviral defense. Oncogene. 2018; 37:5191–204.
https://doi.org/10.1038/s41388-018-0339-4
PMID:29844574

11. Fang Y, Tian S, Pan Y, Li W, Wang Q, Tang Y, Yu T, Wu X, Shi Y, Ma P, Shu Y. Pyroptosis: A new frontier in cancer. Biomed Pharmacother. 2020; 121:109595.
https://doi.org/10.1016/j.biopha.2019.109595
PMID:31710896

12. Latz E, Xiao TS, Stutz A. Activation and regulation of the inflammasomes. Nat Rev Immunol. 2013; 13:397–411.

https://doi.org/10.1038/nri3452 PMID:23702978

13. Ye Y, Dai Q, Qi H. A novel defined pyroptosis-related gene signature for predicting the prognosis of ovarian cancer. Cell Death Discov. 2021; 7:71.
https://doi.org/10.1038/s41420-021-00451-x
PMID:33828074

14. Nagy Á, Munkácsy G, Győrffy B. Pancancer survival analysis of cancer hallmark genes. Sci Rep. 2021; 11:6047.
https://doi.org/10.1038/s41598-021-84787-5
PMID:33723286

15. Wang X, Li M. Correlate tumor mutation burden with immune signatures in human cancers. BMC Immunol. 2019; 20:4.
https://doi.org/10.1186/s12865-018-0285-5
PMID:30634925

16. Yoshihara K, Shahmoradgoli M, Martínez E, Vegesna R, Kim H, Torres-Garcia W, Treviño V, Shen H, Laird PW, Levine DA, Carter SL, Getz G, Stemke-Hale K, et al. Inferring tumour purity and stromal and immune cell admixture from expression data. Nat Commun. 2013; 4:2612.
https://doi.org/10.1038/ncomms3612 PMID:24113773

17. Li T, Fu J, Zeng Z, Cohen D, Li J, Chen Q, Li B, Liu XS. TIMER2.0 for analysis of tumor-infiltrating immune cells. Nucleic Acids Res. 2020; 48:W509–14.
https://doi.org/10.1093/nar/gkaa407 PMID:32442275

18. Li T, Fan J, Wang B, Traugh N, Chen Q, Liu JS, Li B, Liu XS. TIMER: A Web Server for Comprehensive Analysis of Tumor-Infiltrating Immune Cells. Cancer Res. 2017; 77:e108–10.
https://doi.org/10.1158/0008-5472.CAN-17-0307
PMID:29092952

19. Finotello F, Mayer C, Plattner C, Laschober G, Rieder D, Hackl H, Krogsdam A, Loncova Z, Posch W, Wilflingseder D, Sopper S, Ijsselsteijn M, Brouwer TP, et al. Molecular and pharmacological modulators of the tumor immune contexture revealed by deconvolution of RNA-seq data. Genome Med. 2019; 11:34.
https://doi.org/10.1186/s13073-019-0638-6
PMID:31126321

20. Becht E, Giraldo NA, Lacroix L, Buttard B, Elarouci N, Petitprez F, Selves J, Laurent-Puig P, Sautès-Fridman C, Fridman WH, de Reyniès A. Estimating the population abundance of tissue-infiltrating immune and stromal cell populations using gene expression. Genome Biol. 2016; 17:218.
https://doi.org/10.1186/s13059-016-1070-5
PMID:27765066

21. Hinshaw DC, Shevde LA. The Tumor Microenvironment Innately Modulates Cancer Progression. Cancer Res.

2019; 79:4557–66.
https://doi.org/10.1158/0008-5472.CAN-18-3962
PMID:31350295

22. Shulman Z, Stern-Ginossar N. The RNA modification N[6]-methyladenosine as a novel regulator of the immune system. Nat Immunol. 2020; 21:501–12.
https://doi.org/10.1038/s41590-020-0650-4
PMID:32284591

23. Wang L, Zhao W, Hong J, Niu F, Li J, Zhang S, Jin T. Association between IL1B gene and cervical cancer susceptibility in Chinese Uygur Population: A Case-Control study. Mol Genet Genomic Med. 2019; 7:e779.
https://doi.org/10.1002/mgg3.779 PMID:31222982

24. Cui G, Yuan A, Sun Z, Zheng W, Pang Z. IL-1β/IL-6 network in the tumor microenvironment of human colorectal cancer. Pathol Res Pract. 2018; 214:986–92.
https://doi.org/10.1016/j.prp.2018.05.011
PMID:29803656

25. Liu Q, Russell MR, Shahriari K, Jernigan DL, Lioni MI, Garcia FU, Fatatis A. Interleukin-1β promotes skeletal colonization and progression of metastatic prostate cancer cells with neuroendocrine features. Cancer Res. 2013; 73:3297–305.
https://doi.org/10.1158/0008-5472.CAN-12-3970
PMID:23536554

26. Dong GW, Do NY, Lim SC. Relation between proinflammatory mediators and epithelial-mesenchymal transition in head and neck squamous cell carcinoma. Exp Ther Med. 2010; 1:885–91.
https://doi.org/10.3892/etm.2010.124
PMID:22993614

27. Stratakis CA. Cyclic AMP-dependent protein kinase catalytic subunit A (PRKACA): the expected, the unexpected, and what might be next. J Pathol. 2018; 244:257–59.
https://doi.org/10.1002/path.5014
PMID:29205368

28. Kastenhuber ER, Lalazar G, Houlihan SL, Tschaharganeh DF, Baslan T, Chen CC, Requena D, Tian S, Bosbach B, Wilkinson JE, Simon SM, Lowe SW. DNAJB1-PRKACA fusion kinase interacts with β-catenin and the liver regenerative response to drive fibrolamellar hepatocellular carcinoma. Proc Natl Acad Sci USA. 2017; 114:13076–84.
https://doi.org/10.1073/pnas.1716483114
PMID:29162699

29. Shao W, Yang Z, Fu Y, Zheng L, Liu F, Chai L, Jia J. The Pyroptosis-Related Signature Predicts Prognosis and Indicates Immune Microenvironment Infiltration in Gastric Cancer. Front Cell Dev Biol. 2021; 9:676485.
https://doi.org/10.3389/fcell.2021.676485
PMID:34179006

30. Yu P, Zhang X, Liu N, Tang L, Peng C, Chen X. Pyroptosis: mechanisms and diseases. Signal Transduct Target Ther. 2021; 6:128.
https://doi.org/10.1038/s41392-021-00507-5
PMID:33776057

31. Kwon MJ, Rho YS, Nam ES, Cho SJ, Park HR, Min SK, Seo J, Choe JY, Kim ES, Park B, Hong M, Min KW. Clinical implication of programmed cell death-1 ligand-1 expression in tonsillar squamous cell carcinoma in association with intratumoral heterogeneity, human papillomavirus, and epithelial-to-mesenchymal transition. Hum Pathol. 2018; 80:28–39.
https://doi.org/10.1016/j.humpath.2018.03.025
PMID:29634978

32. Pasini FS, Zilberstein B, Snitcovsky I, Roela RA, Mangone FR, Ribeiro U Jr, Nonogaki S, Brito GC, Callegari GD, Cecconello I, Alves VA, Eluf-Neto J, Chammas R, Federico MH. A gene expression profile related to immune dampening in the tumor microenvironment is associated with poor prognosis in gastric adenocarcinoma. J Gastroenterol. 2014; 49:1453–66.
https://doi.org/10.1007/s00535-013-0904-0
PMID:24217965

33. Zeng D, Zhou R, Yu Y, Luo Y, Zhang J, Sun H, Bin J, Liao Y, Rao J, Zhang Y, Liao W. Gene expression profiles for a prognostic immunoscore in gastric cancer. Br J Surg. 2018; 105:1338–48.
https://doi.org/10.1002/bjs.10871 PMID:29691839

34. Xi G, Gao J, Wan B, Zhan P, Xu W, Lv T, Song Y. GSDMD is required for effector CD8^{+} T cell responses to lung cancer cells. Int Immunopharmacol. 2019; 74:105713.
https://doi.org/10.1016/j.intimp.2019.105713
PMID:31276977

35. Wang Q, Wang Y, Ding J, Wang C, Zhou X, Gao W, Huang H, Shao F, Liu Z. A bioorthogonal system reveals antitumour immune function of pyroptosis. Nature. 2020; 579:421–26.
https://doi.org/10.1038/s41586-020-2079-1
PMID:32188939

36. Jorgensen I, Lopez JP, Laufer SA, Miao EA. IL-1β, IL-18, and eicosanoids promote neutrophil recruitment to pore-induced intracellular traps following pyroptosis. Eur J Immunol. 2016; 46:2761–66.
https://doi.org/10.1002/eji.201646647
PMID:27682622

37. Kambara H, Liu F, Zhang X, Liu P, Bajrami B, Teng Y, Zhao L, Zhou S, Yu H, Zhou W, Silberstein LE, Cheng T, Han M, et al. Gasdermin D Exerts Anti-inflammatory Effects by Promoting Neutrophil Death. Cell Rep. 2018; 22:2924–36.
https://doi.org/10.1016/j.celrep.2018.02.067
PMID:29539421

38. Alvarez KL, Beldi M, Sarmanho F, Rossetti RA, Silveira CR, Mota GR, Andreoli MA, Caruso ED, Kamillos MF, Souza AM, Mastrocalla H, Clavijo-Salomon MA, Barbuto JA, et al. Local and systemic immunomodulatory mechanisms triggered by Human Papillomavirus transformed cells: a potential role for G-CSF and neutrophils. Sci Rep. 2017; 7:9002.
https://doi.org/10.1038/s41598-017-09079-3
PMID:28827632

39. Mishalian I, Bayuh R, Levy L, Zolotarov L, Michaeli J, Fridlender ZG. Tumor-associated neutrophils (TAN) develop pro-tumorigenic properties during tumor progression. Cancer Immunol Immunother. 2013; 62:1745–56.
https://doi.org/10.1007/s00262-013-1476-9
PMID:24092389

40. Abakumova TV, Antoneeva II, Gening TP, Gening SO, Dolgova DR, Fomina AV. [Cytokines profile and metabolic activity of neutrophils of peripheral blood when progressing neoplasma]. Patol Fiziol Eksp Ter. 2014; 4:86–90.
PMID:25980232

41. Saleh R, Toor SM, Sasidharan Nair V, Elkord E. Role of Epigenetic Modifications in Inhibitory Immune Checkpoints in Cancer Development and Progression. Front Immunol. 2020; 11:1469.
https://doi.org/10.3389/fimmu.2020.01469
PMID:32760400

42. Rotte A, Jin JY, Lemaire V. Mechanistic overview of immune checkpoints to support the rational design of their combinations in cancer immunotherapy. Ann Oncol. 2018; 29:71–83.
https://doi.org/10.1093/annonc/mdx686
PMID:29069302

43. Velotti F, Barchetta I, Cimini FA, Cavallo MG. Granzyme B in Inflammatory Diseases: Apoptosis, Inflammation, Extracellular Matrix Remodeling, Epithelial-to-Mesenchymal Transition and Fibrosis. Front Immunol. 2020; 11:587581.
https://doi.org/10.3389/fimmu.2020.587581
PMID:33262766

44. D;Eliseo D, Pisu P, Romano C, Tubaro A, De Nunzio C, Morrone S, Santoni A, Stoppacciaro A, Velotti F. Granzyme B is expressed in urothelial carcinoma and promotes cancer cell invasion. Int J Cancer. 2010; 127:1283–94.
https://doi.org/10.1002/ijc.25135
PMID:20027633

45. D'Eliseo D, Di Rocco G, Loria R, Soddu S, Santoni A, Velotti F. Epitelial-to-mesenchimal transition and invasion are upmodulated by tumor-expressed granzyme B and inhibited by docosahexaenoic acid in human colorectal cancer cells. J Exp Clin Cancer Res. 2016; 35:24.
https://doi.org/10.1186/s13046-016-0302-6
PMID:26830472

46. Dufait I, Pardo J, Escors D, De Vlaeminck Y, Jiang H, Keyaerts M, De Ridder M, Breckpot K. Perforin and Granzyme B Expressed by Murine Myeloid-Derived Suppressor Cells: A Study on Their Role in Outgrowth of Cancer Cells. Cancers (Basel). 2019; 11:808.
https://doi.org/10.3390/cancers11060808
PMID:31212684

47. Wang X, Wang HK, Li Y, Hafner M, Banerjee NS, Tang S, Briskin D, Meyers C, Chow LT, Xie X, Tuschl T, Zheng ZM. microRNAs are biomarkers of oncogenic human papillomavirus infections. Proc Natl Acad Sci USA. 2014; 111:4262–67.
https://doi.org/10.1073/pnas.1401430111
PMID:24591631

48. Li S, Yang F, Wang M, Cao W, Yang Z. miR-378 functions as an onco-miRNA by targeting the ST7L/Wnt/β-catenin pathway in cervical cancer. Int J Mol Med. 2017; 40:1047–56.
https://doi.org/10.3892/ijmm.2017.3116
PMID:28902356

49. Zhou C, Chen Z, Peng C, Chen C, Li H. Long Noncoding RNA TRIM52-AS1 Sponges miR-514a-5p to Facilitate Hepatocellular Carcinoma Progression Through Increasing MRPS18A. Cancer Biother Radiopharm. 2021; 36:211–19.
https://doi.org/10.1089/cbr.2019.3271
PMID:32391716

50. Liu Y, Wu Y, Liu S, Dai Y. Long Non-Coding RNA TRIM52-AS1 Promotes Growth and Metastasis via miR-218-5p/ROBO1 in Hepatocellular Carcinoma. Cancer Manag Res. 2021; 13:547–58.
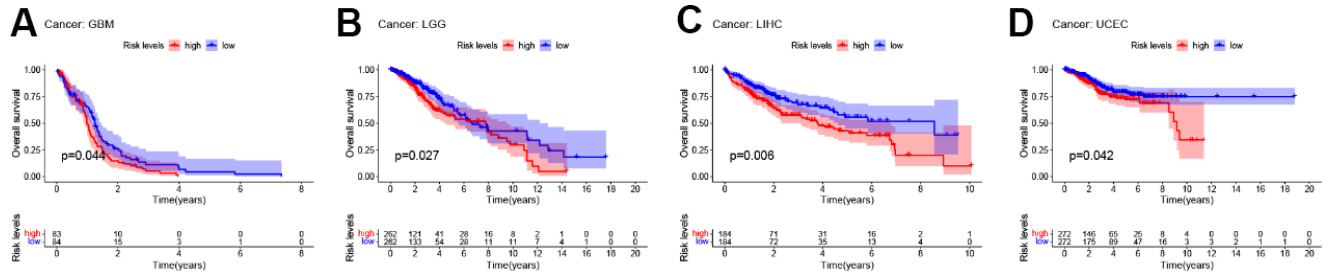https://doi.org/10.2147/CMAR.S286205
PMID:33519234
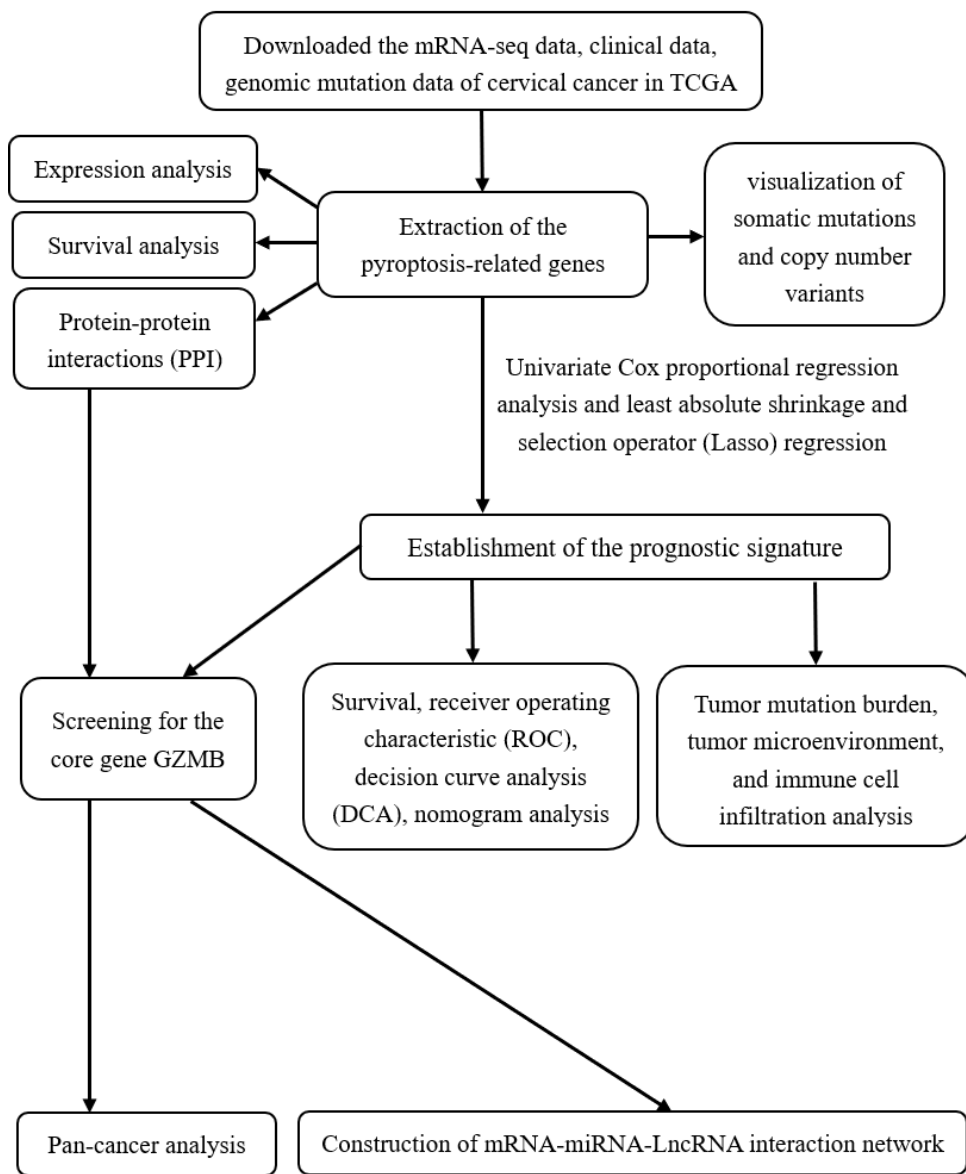
**Supplementary Figure 1. Study flow diagram.**
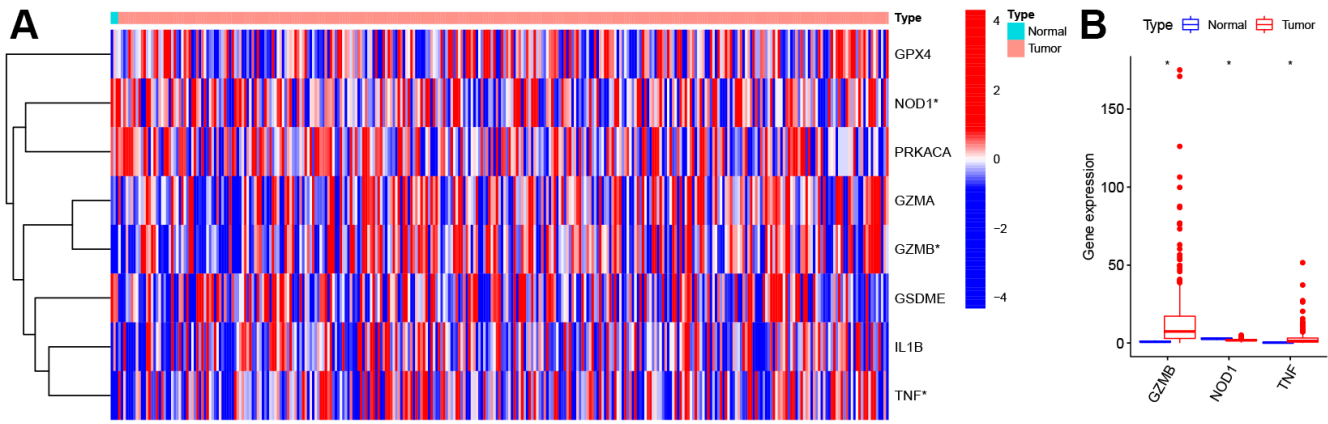
Supplementary Figure 2. Prognostic pyroptosis-related genes. (**A**) Heatmap. (**B**) Boxplot. Compared to normal cervical tissues, GZMB and TNF are highly expressed in cervical cancer tissues, while NOD1 is lowly expressed. *p < 0.05, **p < 0.01, and ***p < 0.001.

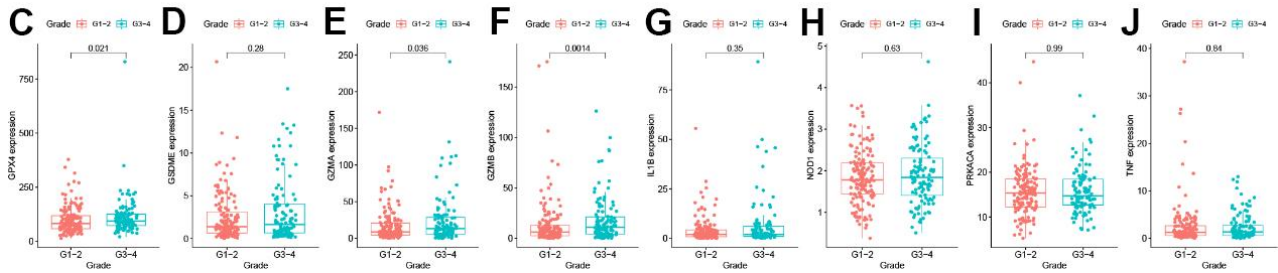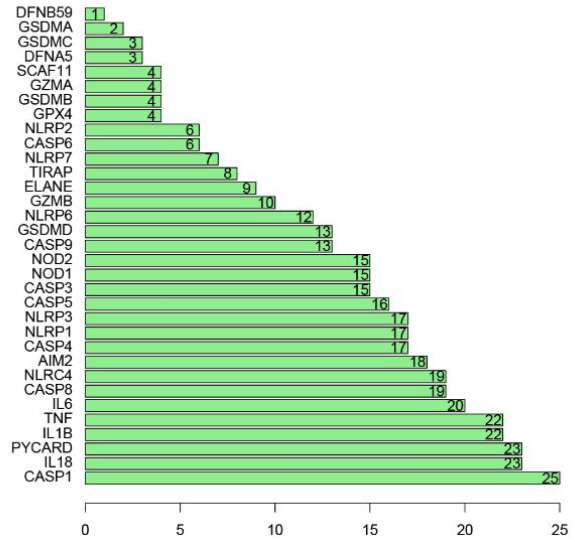**Supplementary Figure 3. The pyroptosis-related signature in other tumors.** Kaplan-Meier curves showed lower overall survival rates in the high-risk group than in the low-risk group in GBM (**A**), LCG (**B**), LIHC (**C**), and UCEC (**D**) (P < 0.05). GBM, Glioblastoma multiforme. LGG, Brain Lower Grade Glioma. LIHC, Liver hepatocellular carcinoma. UCEC, Uterine Corpus Endometrial Carcinoma.
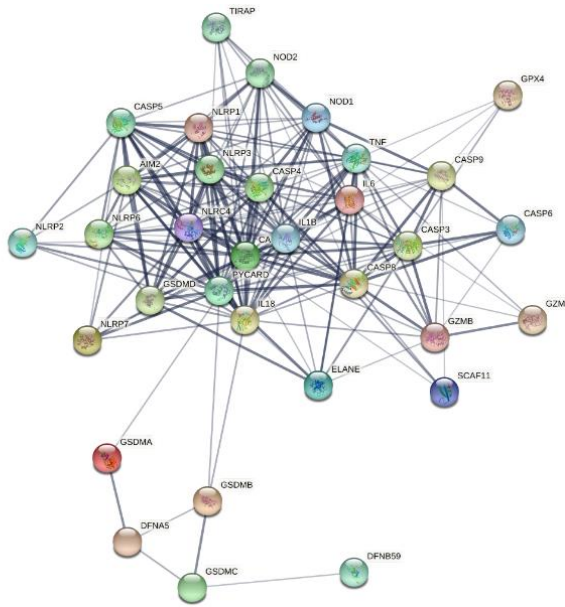
Supplementary Figure 4. Identify the core gene of the pyroptosis-related signature. (**A**) PPI network of the PRGs. (**B**) The degree of binding of PRGs. (**C–J**) Correlation of genes of the pyroptosis-related signature with the clinical feature Grade. The expression of GPX4, GZMA, and GZMB was significantly higher in the G3-4 group. PRGs, Pyroptosis-related genes.

Supplementary Tables

Supplementary Table 1. Detailed list of pyroptosis genes.

Gene	Full-names
AIM2	Absent in melanoma 2
CASP1	cysteine-aspartic acid protease-1
CASP3	cysteine-aspartic acid protease-3
CASP4	cysteine-aspartic acid protease-4
CASP5	cysteine-aspartic acid protease-5
CASP6	cysteine-aspartic acid protease-6
CASP8	cysteine-aspartic acid protease-8
CASP9	cysteine-aspartic acid protease-9
ELANE	elastase, neutrophil expressed
GPX4	glutathione peroxidase 4
GSDMA	gasdermin A
GSDMB	gasdermin B
GSDMC	gasdermin C
GSDMD	gasdermin D
GSDME/DFNA5	gasdermin E
GZMA	granzyme A
GZMB	granzyme B
IL18	interleukin 18
IL1B	interleukin 1 beta
IL6	interleukin 6
NLRC4	NLR family CARD domain containing 4
NLRP1	NLR family pyrin domain containing 1
NLRP2	NLR family pyrin domain containing 2
NLRP3	NLR family pyrin domain containing 3
NLRP6	NLR family pyrin domain containing 6
NLRP7	NLR family pyrin domain containing 7
NOD1	nucleotide binding oligomerization domain containing 1
NOD2	nucleotide binding oligomerization domain containing 2
PJVK	pejvakin/deafness, autosomal recessive 59
PLCG1	phospholipase C gamma 1
PRKACA	protein kinase cAMP-activated catalytic subunit alpha
PYCARD	PYD and CARD domain containing
SCAF11/SFRS2IP	SR-related CTD associated factor 11
TIRAP	TIR domain containing adaptor protein
TNF	tumor necrosis factor

Supplementary Table 2. Detailed list of pan-cancer names.

Cancer type	Full-names
ACC	Adrenocortical carcinoma
BLCA	Bladder Urothelial Carcinoma
BRCA	Breast invasive carcinoma
CESC	Cervical squamous cell carcinoma and endocervical adenocarcinoma
CHOL	Cholangiocarcinoma
COAD	Colon adenocarcinoma
COADREAD	Colon adenocarcinoma/Rectum adenocarcinoma Esophageal carcinoma
DLBC	Lymphoid Neoplasm Diffuse Large B-cell Lymphoma
ESCA	Esophageal carcinoma
FPPP	FFPE Pilot Phase II
GBM	Glioblastoma multiforme
GBMLGG	Glioma
HNSC	Head and Neck squamous cell carcinoma
KICH	Kidney Chromophobe
KIPAN	Pan-kidney cohort (KICH+KIRC+KIRP)
KIRC	Kidney renal clear cell carcinoma
KIRP	Kidney renal papillary cell carcinoma
LAML	Acute Myeloid Leukemia
LGG	Brain Lower Grade Glioma
LIHC	Liver hepatocellular carcinoma
LUAD	Lung adenocarcinoma
LUSC	Lung squamous cell carcinoma
MESO	Mesothelioma
OV	Ovarian serous cystadenocarcinoma
PAAD	Pancreatic adenocarcinoma
PCPG	Pheochromocytoma and Paraganglioma
PRAD	Prostate adenocarcinoma
READ	Rectum adenocarcinoma
SARC	Sarcoma
SKCM	Skin Cutaneous Melanoma
STAD	Stomach adenocarcinoma
STES	Stomach and Esophageal carcinoma
TGCT	Testicular Germ Cell Tumors
THCA	Thyroid carcinoma
THYM	Thymoma
UCEC	Uterine Corpus Endometrial Carcinoma
UCS	Uterine Carcinosarcoma
UVM	Uveal Melanoma